Microporous and Mesoporous Materials 323 (2021) 111168

Contents lists available at ScienceDirect

Microporous and Mesoporous Materials

journal homepage: www.elsevier.com/locate/micromeso

Formation of carbon nanofibers with Ni catalyst supported on a micro-mesoporous glass

M.A. Mazo [a,*], J. Sanguino [a,b], I. Martín-Gullón [c], J. Rubio [a]

[a] Instituto de Cerámica y Vidrio, CSIC. C/ Kelsen 5, 28049, Madrid, Spain
[b] Instituto de Genética Médica y Medicina Molecular, Hospital La Paz, P° de la Castellana 261, 28046, Madrid, Spain
[c] Chemical Engineering Department, University of Alicante, 03690, Alicante, Spain

ARTICLE INFO

Keywords:
Catalytic chemical vapor deposition
Carbon nano fibers
Vycor process
CNFs/glass materials
Ni/SiO_2 catalyst/support system

ABSTRACT

The Ni/SiO_2 system is one of the most interesting to produce CO_x-free H_2 and valuable carbon nanofibers (CNFs) by the catalytic decomposition of CH_4. SiO_2 is one of the most effective support while Ni catalyst displays long life and high activity. We studied the catalytic chemical vapor deposition (CCVD) process of CH_4 within Ni/glass system at relatively low temperature (600 °C) during long times (3 h), varying the amount of the catalyst (2.3–17.8% Ni(%)) and the carbon source (100:200 to 100:0, CH_4:N_2). As the amount of Ni and CH_4 increases, the formation of CNFs is enhanced giving as a result CNFs/glass materials with more amount, longer and thicker CNFs.

The initial microstructure of the glass support and the way of Ni catalyst is deposited play a decisive role. Pristine porous glass displays a microstructe of interconnected mesopores which are progressively filled with Ni, producing *ink-bottle* pores with open ends. After the CCVD process as the amount of Ni or CH_4 increases, the porosity of the Ni-doped glass is reduced due to the progressively filling of the mesopores (4 nm) with CNFs. Furthermore, due to the formation of large entanglements of CNFs new pores appear (20–70 nm) depending on the processing conditions. *Fish-bone* with hollow core and *bamboo*-like CNFs are found over the surface and also inside the porous glass support. It is observed a base-growth mechanism due to the strong interaction between the catalyst and the support, which prevents the Ni deactivation enhancing its activity for long times.

1. Introduction

Carbon nanomaterials (CNs) such as carbon nanotubes (CNTs), carbon nanofibers (CNFs) and also opened CNs have received much attention since the publication of *Ijima's* works [1,2]. CNs display a very high aspect ratio, very high theoretical mechanical properties (*Young's* module, flexural and bending strength, toughness, etc.), high electrical and thermal conductivities which offer excellent properties as reinforcing agents giving many opportunities and applications in the composites field among others [3–8]. Many studies have been done using polymeric matrices [4,9], but an increasing interest is observed in metal [10] and ceramic matrices [3,5,11]. However, CNs/ceramic composites have not achieved the expected properties, due basically to the tendence of the CNs to agglomerate preventing a satisfactory CNs dispersion in the matrix generating an inadequate CNs/matrix interphase. CNs/glass composites, included inside the ceramic matrix composites, display a large amount of applications in different fields such as photonic [12], electromagnetic shielding [13], catalyst [14], biocatalyst [15], removal of contaminants in wastewater [16], filters [17], etc. Besides, the use of a glass matrix reduces the sintering temperature, limits the thermal degradation of the reinforcement and also saves energy [18]. The first attempt to produce CNTs/glass composites included a simple mixture and consolidation processes. The promising composites displayed large agglomerates of CNTs [19] leading to a poor matrix-reinforcement interphase. Afterwards, many efforts have been made to solve this problem and, the proposed solutions included sonication, use of surfactants, purification and subsequent functionalization of CNs and the employment of the sol-gel method which enhances the dispersion and improves the interaction between the matrix and the reinforcement, [20–22]. All of these processes make the route longer, more expensive and also include impurities which can directly affect the sintering process and the final properties of the composites. Other methods include the traditional ceramic processing with powerfull milling techniques and subsequent sintering [18,23]. An alternative method is the *in situ*

* Corresponding author.
E-mail address: sandra@icv.csic.es (M.A. Mazo).

https://doi.org/10.1016/j.micromeso.2021.111168
Received 2 March 2021; Received in revised form 20 April 2021; Accepted 10 May 2021
Available online 20 May 2021

growth of CNs (CNFs, CNTs and graphene) by the catalytic chemical vapor deposition (CCVD). The CNs are homogenously formed directly inside the ceramic matrix, avoiding the dispersion steps and furthermore CCVD process is relatively simple, cheap and scalable which can be used to many supports [3,24]. First experiments were carried out employing metallic catalyst (Fe, Co and Fe/Co alloys) supported over metal oxides (Al_2O_3, MgO and $MgAl_2O_4$) [25,26]. There are many parameters that have to be determined in order to obtain optimal results in the CCVD proccess. These factors include the selection and control of the metal catalyst (the amount, type and size of crystal), the reduction treatment of the catalyst, the temperature and duration of the thermal treatment, the carbon source (type and composition), etc. [27–29]. Usually transition metals (Ni, Fe and Co) are the most popular employed to produce CNs. Ni catalyst presents higher catalytic activity than other metals (Co and Fe), but it is limited to low temperature because is rapidly deactivated above 600 °C [30]. The use of supported bimetallic transition metal catallyst (Ni, Fe, Co) offers new possibilities enhancing the catallytic activity during longer times preventing its passivation [27,30–33]. Many supports can be used such as SiO_2, Al_2O_3, MgO, TiO_2, ZrO_2, etc. [24]. Currently, the study of interactions between the catalyst and support and also the mechanism of the formation of the CNs is a very important issue [30,31]. Generally, as carbon source can be employed gaseous (methane, ethylene, acetylene, CO, etc.) or liquid (toluene, benzene, xylene, alcohol, etc.) carbon compounds. Nowadays, the employ of metane offers the benefit of production $CO_{x\text{-free}}$ H_2, highly demanding these days as green energy source and a very promising material to be used as low temperature fuel cell, futhermore natural gas is cheap and abundant. Currently, several groups are focused in the study of the behavior of mono or bimetallic transition metals (Ni, Fe, Co) supported over SiO_2 and TiO_2–Al_2O_3 [30,33], being the Ni/SiO_2 system one of the most effective [27].

In a previous work, we developed CNFs/glass materials by the *in situ* growth of CNFs in a porous glass employing CH_4 as carbon source and Ni as catalyst varing the temperature and dwelling time of the CCVD process. It was stablished 600 °C and 3 h of reaction time [34] as the best reaction parameters. In this new paper, we studied another key paramethers of the CCVD process as the Ni amount and the CH_4:N_2 ratio. The micro/mesoporous glass support was obtained through a variation of the *Vycor* process applied over a SiO_2/B_2O_3/Na_2O glass [35–39]. This process is based on a thermal phase separation of the pristine glass followed by a selective HCl leaching of the B_2O_3–Na_2O soluble glass phase that allows to control the pore size of the final SiO_2-rich glass matrix. A homogenous dispersion of the catalyst (i.e. $NiAc_2$) is deposited over the surface and inside of the micro/mesopores of the glass support and finally, the CCVD process produces the *in situ* growth of CNFs homogenously dispersed all over the support, including the surface and inside of the pores.

The aim of this work is to study the influence of the amount of catalyst (Ni(%)) and the carbon source (i.e. CH_4:N_2 ratio), the last one rarely studied in the literature [29]. The influence of the porous microstructure of the glass support during the different steps of that process is a very important issue which must be taken into consideration. Our results demonstrate that the amount of the catalyst (Ni(%)) and carbon source (CH_4:N_2 ratio) deeply influence both the yield and order degree of the CNFs produced after the CCVD process. It is well-known, that the carbon reinforcements increase both electrical and thermal properties of the related composites [11]. Based on this fact, the experimental conditions have been choosen in order to obtain the maximum amount of CNFs. All those findings have made it possible to know the mechanism of the CNFs growth in the pores of the glass support.

2. Experimental methods

2.1. Catalytic deposition

Glass with a nominal weight composition 50/40/10 of SiO_2/B_2O_3/Na_2O was prepared by the conventional melting proccess at 1450 °C (2 h) employing a Pt crucible. Glass was heated at 680 °C during 3 h to induce the phase separation, then it was ground and sieved between 200 and 300 μm and the particles were leached in an aqueous solution of HCl 10% at 95 °C for 20 h. A porous glass was obtained with a BET surface area (S_{BET}) of 185 m^2g^{-1}, total pore volume of meso and micropores ($V_{mic\ +\ mes}$) of 0.41 cm^3g^{-1} and chemical composition of 93.2/6.3/0.4 (wt.%) of SiO_2/B_2O_3/Na_2O [34].This porous glass was impregnated with an aqueous solution of nickel acetate ($NiAc_2$) at 90 °C for 48 h. Then the sample was washed with water several times and dried for 24 h at 180 °C. In order to determine the role of the amount of nickel in the *in situ* formation of CNFs, four different solutions were studied: 0.02 M, 0.04 M, 0.1 M and 0.2 M. The porous glass samples with Ni deposited were named as Ni-0.02, Ni-0.04, Ni-0.1 and Ni-0.2, respectively.

2.2. CNFs growth

CNFs were grown inside the porous glass by the CCVD process. In a typical preparation, the glass was first impregnated with $NiAc_2$ and then was heated with a continuous flow of CH_4:N_2 in an alumine tubular furnace at 600 °C during 3 h (heating and cooling rates, 10 °$Cmin^{-1}$). The sample with the highest concentration of $NiAc_2$ (i.e. Ni-0.2) was selected to study the influence of the CH_4:N_2 ratio during the formation of CNFs. Five different flows of CH_4:N_2 were performed 100:200, 100:100, 100:50, 100:25 and 100:0 ratio (vol/vol) using a total flow in all the cases of 180 cm^3min^{-1}. N_2 was employed as carrier gas and, also to ensure an inert ambient inside the tubular furnace, while CH_4 was used as carbon source. The related samples were named as CN 100:200, CN 100:100, CN 100:50, CN 100:25 and CN 100:0, respectively.

Besides, all the Ni-impregnated/glass compositions (Ni-0.02, Ni-0.04, Ni-0.1 and Ni-0.2) were heated under a CH_4:N_2 flow (100:100, vol/vol) to study the influence of the Ni content in the CNFs formation. The resulted CNFs/glass samples were named as CN-0.02, CN-0.04, CN-0.1, CN-0.2, respectively.

2.3. Characterization techniques

Elemental analysis was carried out with an Inductively Coupled Plasma Optical Emission spectrometer (IRIS Advantage, Thermo Jarrell Ash Corp, USA) to determine Ni(%), Si(%) and B(%) and by an elemental carbon analyzer (CS-200, LECO Corp., USA) to measure the C(%). Microstructural analysis were carried out by Field Emission Scanning Electron Microscopy technique (FE-SEM) employing a Hitachi S-4700 microscope operating at 20 keV and High Resolution Transmission Electron Microscopy (HR-TEM) using a Jeol JEM-2010 microscope operating at 200 kV. Selected areas of Ni/SiO_2 samples were examined with FE-SEM by Energy Dispersive X-ray analysis (EDX, Noran System Six, Thermo Fisher Scientific, USA) via mapping or elemental analysis of Ni. In order to complete the microstructural study, the porosity of glass and CNFs/glass materials was evaluated by N_2 adsorption-desorption isotherms, employing a TriStar 3000 instrument (Micromeritics Corp., USA). The S_{BET} area was determined by the *Brunauer, Emmett and Teller* equation [40]. The *Barret, Joyner and Halenda* (BJH) method [41] was carried out to obtain the mesopore size distributions (PSDs), employing the adsorption branch of the isotherm. Mesopore surface areas (S_{mes}), volume (V_{mes}) and average pore diameter (d_{pore}) were also calculated assuming cylindrical pores. Micropores, volume (V_{mic}) and surface (S_{mic}), were analysed with the *t-plot* method [42] applying *Harkins-Jura* equation [43]. V_{mic} was calculate subtracting V_{mes} from the total volume ($V_{mic\ +\ mes}$) measured at $p/p^o = 0.99$. Additionally, the volume related to macropores (V_{macro}) was calculated subtracting the pore volume

determined by He picnometry (AccuPyc 1330, Micromeritics Corp., USA) from $V_{mic\ +\ mes}$. The surface area related to Ni catalyst (S_{Ni}) was calculated by the subtraction of S_{BET} related to original glass and the S_{BET} after Ni deposition. Raman measurements of the CNFs/glass materials were carried out in a InVia Raman spectrometer (Renishaw plc., UK) equipped with a 514 nm Ar^{+} laser. The evolution of the in-plane lateral domain size of carbon nanoclusters (L_a) was calculated by equation (1) [44],

$$I_D/I_G = C(1)/L_a(nm) \quad (1)$$

where C(1) is a constant which acquires a value of 4.4 when a 514 nm laser is used. Thermal analysis was done with a thermogravimentric instrument (SDT Q600 TA Instruments, USA) from R.T. to 1000 °C under flowing air with a heating rate of 10 °Cmin^{-1}. Infrared spectra in the Attenuated Total Reflectance mode (ATR) were obtained conecting a MIRacleTM ATR device to a Fourier Transform Infrared (FT-IR) spectrometer (BX, PerkinElmer Corp., USA).

3. Results and discussion

It is well-known that the main variables for the CNFs growth in the CCVD process are the catalyst, carbon source, thermal treatment and its duration. In a previous work [34] and taking into account our experimental conditions, we stated that the optimal heat treatment for the CNFs growth was 600 °C and 3 h of holding time. Therefore, in this new work we have studied the influence of the amount of the metallic catalyst (i.e. concentration of $NiAc_2$) and the carbon source concentration. In the case of the catalyst amount, the concentration of $NiAc_2$ was varied from 0.02 M to 0.2 M keeping constant the rest of the parameters (i.e. CH_4:N_2 ratio 100:100 at 600 °C (3 h)).

3.1. Influence of Ni amount

Fig. 1 shows the elemental mapping of Ni for Ni/SiO_2 samples with different amount of catalyst. The catalyst is homogenously dispersed all over the material surface. Although the size of catalyst is rather similar in all the cases, the coalescence of several particles can be detected in the samples with the highest amount of Ni (i.e. Ni-0.1 and Ni-0.2). As can be clearly observed in Table 1 and Fig. 1, there is a good agreement between the Ni(%) (obtained by both elemental analyst and EDX) and the mapping images.The FE-SEM micrographs (Fig. 2) of these samples, reveal some voids and porosity, generated during the HCl leaching due to the removing of the B_2O_3–Na_2O soluble phase. On the other hand, the filling of those voids and pores is observed steadily as the amount of Ni (%) increases. The presence of some cracks is also appreciated for the sample with the highest Ni(%), probably due to the large amount of Ni deposited over the surface and inside the pores of the glass support.

The influence of the amount of Ni catalyst for the CNFs formation is

Table 1
Ni (%) (determined by elemental analyst (Ni(%) and EDX (Ni_{EDX}(%)), C (%), CNFs diameter and volume related to macropores (V_{macro}) for the Ni-impregnated glasses and CNFs/glass materials obtained with different concentration of $NiAc_2$ at 600 °C (3 h) and 100:100 of CH_4:N_2 ratio.

Sample	Ni $(AcO)_2$ (M)	Ni (%)	Ni_{EDX}(%)	C (%)	CNF diameter (nm)	V_{macro}(cm^3g^{-1})
CN-0.02	0.02	2.3	0.7	2.2	–	0.09
CN-0.04	0.04	4.4	1.2	2.2	–	0.29
CN-0.1	0.1	9.9	8.2	6.4	24 ± 6	0.11
CN-0.2	0.2	17.8	18.8	8.0	27 ± 6	0.14

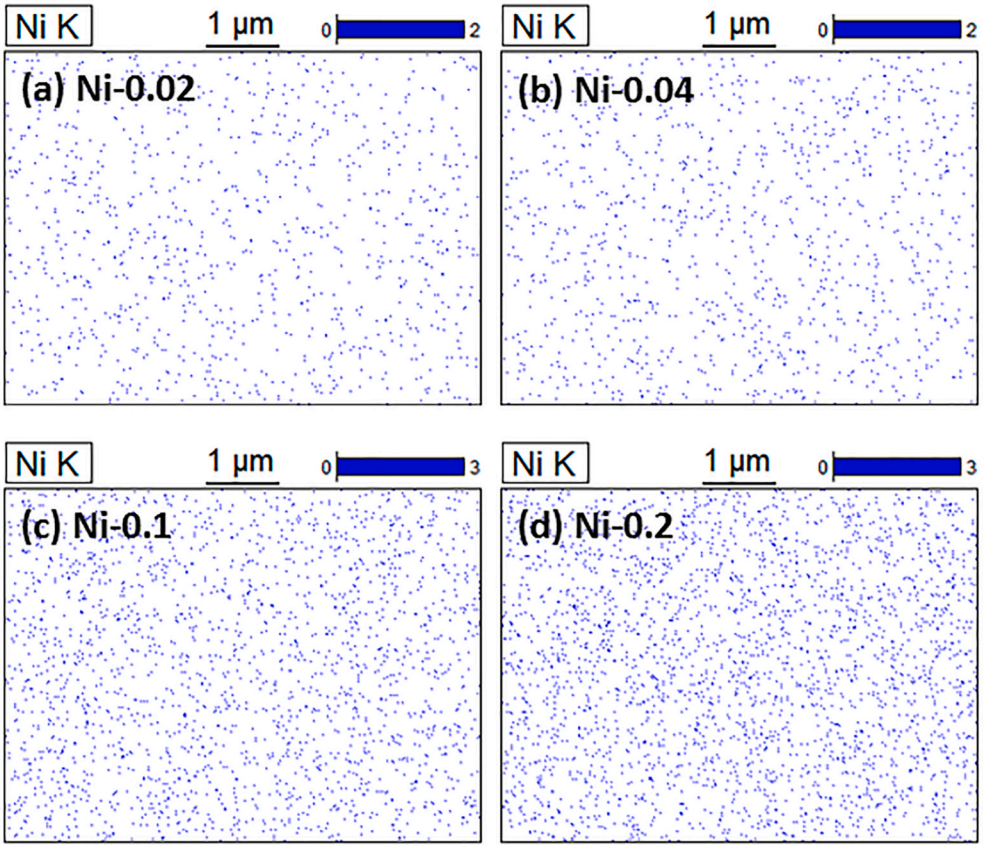

Fig. 1. FE-SEM mapping of Ni of Ni/SiO_2 materials impregnated with different Ni(%): (a) Ni-0.02, (b) Ni-0.04, (c) Ni-0.01 and (d) Ni-0.02.

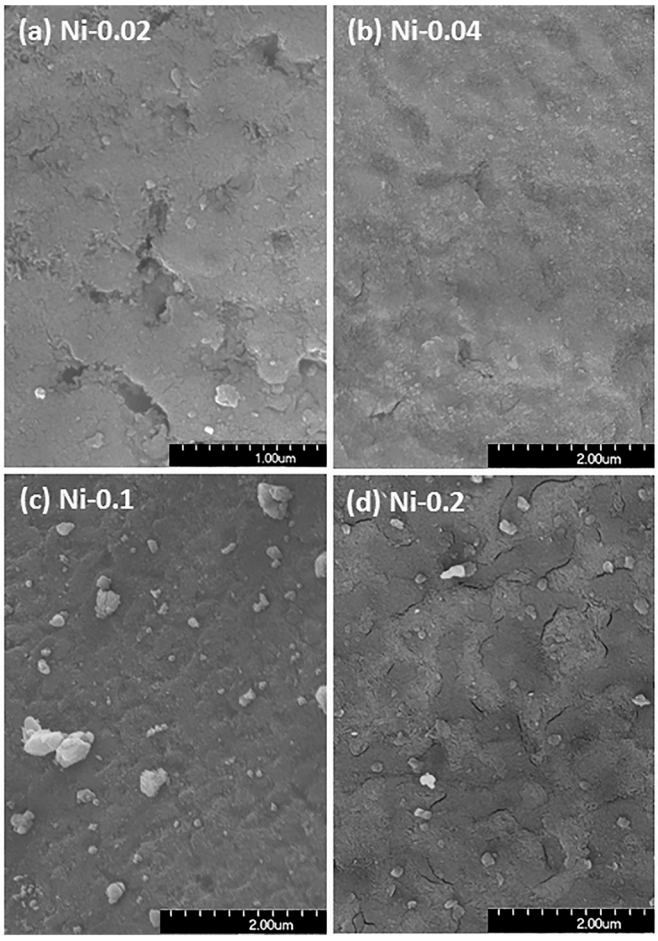

Fig. 2. FE-SEM micrographs of Ni/SiO_2 materials impregnated with different Ni(%): (a) Ni-0.02, (b) Ni-0.04, (c) Ni-0.01 and (d) Ni-0.02.

given in Table 1 where is observed that the C(%) increases with the amount of Ni. *Takenaka* et al. [27] indicated that the activity and catalytic life of Ni for the CH_4 decomposition increase with the Ni(%) in the range from 1 to 40%, but higher amounts (>50%) reduce both the activity and catalytic life.

FE-SEM micrographs showed in Fig. 3(a–d) are in line with the results presented in Table 1 and Fig. 2 displaying great differences depending on the Ni(%). The samples with the lowest Ni(%) (i.e. CN-0.02 and CN-0.04) show very short (<500 nm) and only few CNFs which do not agree with the C(%) (≈2%, Table 1). The observed CNFs emerge from the glass support, so the majority of the CNFs could be hidden inside the porous network. On the other hand, the samples with the highest Ni(%) present homogeneous and well-dispersed entaglements of CNFs all over the glass surface coming from the porous glass network, being this fact especially noticeable in the CN-0.2 sample. The CNFs observed in the CN-0.1 sample are short (<0.1 μm) with a mean diameter of 24 nm, while in the case of CN-0.2, the CNFs are longer (from 1 to several μm) with a slightly broader diameter of 27 nm. As it was observed by *Shokry* et al. [31], the presence of a minimum amount of catalyst seems to be absolutely necessary to obtain CNFs in the porous glass, increasing both length and quantity with the Ni(%).

The sample with the highest amount of carbon (CN-0.2) was also observed by means of TEM and HR-TEM (Fig. 3 (e)–(j)). As it was previously stated, both CNFs and CNTs can be formed by CH_4 decomposition employing the Ni/SiO_2 system [27,34]. In the present case, there are mostly observed *bamboo-like* (diameter 10–20 nm, Fig. 3(g)) and *fish-bone* with hollow core CNFs (diameter <20 nm, Fig. 3 (h)) where graphitic planes are stacked at a certain angle to the axis of the fibres. The Ni particles are spherical in shape with a mean size <5 nm (Fig. 3 (f–h)), and they are observed apparently inside the CNFs but not at the tips. It is important to note how several Ni particles appear very close indicating the coalescence of the catalyst in these experimental conditions (Fig. 3(e), (f) and (h)) which is in accordance with mapping results (Fig. 1(d)). Several authors observed how as the concentration of Ni increased more active Ni sites appeared and, those sites were well-dispersed all over the porous glass support enhancing the carbon deposition [27,28,32]. Furthermore, it is also observed an increase of the CNFs diameter with the Ni (%) (Table 1), which is directly related to the coalescence of the Ni particles during the heat treatment [45] (Fig. 3 (h)). Additionally, in Fig. 3(i–j) is observed the coalescence of a group of spherical Ni particles (Ni (111) lattice planes spaced ≈0.2 nm) surrounded by CNFs (C (002) with lattice planes spaced ≈0.3 nm). The crystallographic concurrence observed between Ni (111) and C (002) planes is essential for the CCVP process and the growth of CNFs [46]. The CNFs show open edges on their outer surface and, that fact produces a high chemical activity that could be interesting in medical and other applications, *as Miniach* et al. [28] indicated. Also, it can be clearly observed how these Ni particles are homogenously distributed and placed on the glass support and rarely inside the CNFs. This fact indicates a very strong interaction due to the chemical affinity [31] between the glass support and the catalyst particles which also implies that the base growth mechanism prevails [33]. The *bamboo*-like structure defects are usually observed in the CNTs produced by a base growth mechanism [31].

The evolution of the material porosity has been followed by means of N_2 adsorption-desorption measurements, He pycnometry and FE-SEM images. The changes in porosity due to the *in situ* growth of CNFs can not be understood without knowing the porosity of the pristine Ni impregnated porous glasses (Fig. 4(a), (b) and Table 2) and, also the effect of the thermal treatment in such porosity. As it was reported in a previous work [34], the as prepared glass was non-porous but after the acid leaching a porous glass was formed. The glass displayed a type IVa isotherm with a H3 hysteresis loop, which mainly corresponds to a mesoporous material with a wide range of pore sizes [47]. Those pores were cylindrical in shape and open at both ends. The pore size diameter varied from 2 to 150 nm. As it is expected, the support porosity changed when is impregnated with $NiAc_2$ and those changes greatly depend on the Ni(%) (Fig. 4(a) and (b)). The sample with the smallest Ni(%) resembles to the pristine porous glass [34] but, as the Ni(%) increases the shape of isotherm changes and, althought in all the cases the isotherms are type IVa, the hyteresis loops progressively change from H3 to H4 and, finally to H2 type. The H3 loop of the Ni-0.02 sample could indicate a microstructure of non-rigid aggregates with the contribution of macropores [47]. The Ni-0.04 sample presents a H4 hysteresis loop, similar to H3, but also indicates the presence of micropores [47]. The Ni-0.1 and Ni-0.2 samples display H2b and H2a type loops, respectively, which are associated to pore blocking in *ink-bottle* pores and, where their pore neck distribution is very large (H2a) or very narrow (H2b) [47]. In summary, the $NiAc_2$ deposition can occur as follows: in the case of the lowest Ni (%), the $NiAc_2$ can pass thoughtout the open interconnected pore structure filling all the wide range of pores, as consequence, the porosity parameters decrease and the pore diameter shifts to a lower value (i.e. from 18.7 to 10.1 nm, Table 2)). As the amount of Ni increases (for the Ni-0.04 sample) the open mesoporous microstructure continues filling, the mesopores of around 10 nm disappear generating a bimodal PSDs with smaller and bigger mesopores and also some micropores. The porosity parameters decrease except the ones related to micropores wich experience a little increase (Table 2). In the cases of the Ni-0.1 and Ni-0.2 samples a different behaviour is observed. It seems clear that the open porous microstructure turns into *ink-bottle* pores with open ends. For Ni-0.1, a wide distribution of necks is obtained, with a bimodal PSD with pores centred of around 6 and 60 nm. But finally, for Ni-0.2, the biggest pores are completely filled and, as consecuence the size of necks moves to lower values (4.1 nm). The filling of large mesopores produces

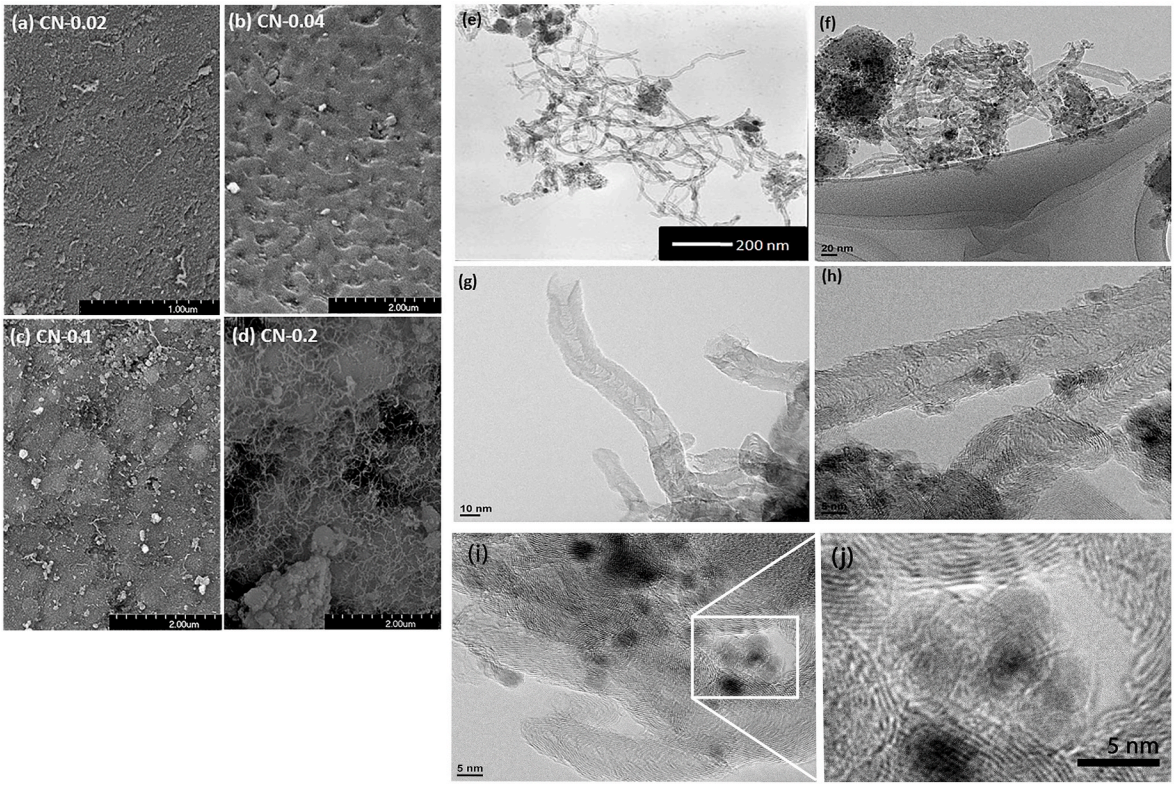

Fig. 3. FE-SEM micrographs of CNFs/glass materials obtained with different Ni(%): (a) CN-0.02, (b) CN-0.04, (c) CN-0.1 and (d) CN-0.2 at 600 °C (3 h) under a current flow of CH_4:N_2 100:100. (e) TEM and (f)–(j) HR-TEM micrographs of CN-0.2 sample with different magnifications.

a decrease in their size and transforms them into small pores leading to an increase in the porosity parameters (Table 2). Finally, the FE-SEM images (Fig. 2) of these samples reveal the presence of some macroporosity that was determined by He pycnometry (Table 1). The V_{macro} increases with the amount of Ni(%) probably ascribed to a higher deposition of the catalyst.

After the thermal treatment in CH_4:N_2 atmosphere, the shape of isotherms and hysteresis loops are maintained in all the cases (Fig. 4(c) and (d)). The isotherm of the CN-0.02 sample, with the smallest amount of Ni(%), practically does not change revealing a low amount of CNFs formed. The other samples display a moderate decrease on the adsorbed volume associated with the formation of CNFs. In those samples, as the Ni(%) increases S_{BET}, S_{mes}, V_{mes} are drastically reduced due to the filling of mesopores by the formation of CNFs while S_{mic} and V_{mic} remain more or less constant (Table 2). This could indicate that Ni particles are located mainly inside mesopores and in a lesser extent within the micropores due to their smaller size. Additionally, S_{Ni} is only noticeable in the samples with the highest Ni(%) (33 and 101 m^2g^{-1} for Ni-0.1 and Ni-0.2 samples, respectively). Those data perfectly agree with both the C (%)(Table 1) and the FE-SEM micrographs (Fig. 3(a)–(d)). It is also important to notice in the samples with the highest Ni(%) (CN-0.1 and CN-0.2, Fig. 4 (d)) the presence of pores centred at around 60–70 nm, that are assigned to new pores formed by large entanglements of CNFs grown on the surface but also inside of the pores of the support [34,48]. The thermal process in air at 600 °C only produces the beginning of sintering leading to a little decrease of S_{BET}, due to the removing of some of the smallest pores which sinter at lower temperatures [38]. S_{mic} and V_{mic} decrease while S_{mes} and V_{mes} remain practically without changes (Table 2). In summary, when a CH_4:N_2 flow is used, apart from a slightly variation due to the beginning of sintering, the majority of changes that occurr in the porosity are due to the formation of CNFs within the porous microstructure of the glass support. As the Ni(%) increases the S_{BET}, S_{mes} and V_{mes} values radically decrease as consecuence of the progressive filling of the mesopores located inside of the porous support, but also another porosity is found related to large entanglements of CNFs formed in the glass support (i.e. 60-70 nm pores). In conclusion, the porosity of the CNFs/glass materials can be controlled by the Ni(%) since it determines the amount, length and diameter of formed CNFs which are directly related with the porosity of the material.

As it was proposed elsewhere [49] the difference between the S_{BET} of the these final materials and the Ni-impregnated glass support treated at high temperature in air (i.e. 900 °C; ΔS_{BET} = S_{BET} sample-S_{BET}-900 °C-Air) could be used as a first estimation of the bundles of carbon formed. ΔS_{BET} divided by the amount of the carbon formed (ΔS_{BET}/C(%)) also indicates the features of the deposited carbon and, in this sense low values indicate smaller diameter and lower amount of carbon deposited in tubular form [49]. Based on those asumptions, it seems clear how as the Ni(%) increases the ΔS_{BET}/C decreases (Fig. 5) which perfectly agrees with the evolution of the CNFs diameter (Table 1). However, due to the great differences in terms of the quantity of obtained CNFs other information must be taken into account in order to determine the optimal experimental conditions.

Fig. 6 collects the Raman spectra of the CNFs/glass materials obtained varing the Ni(%). In all the cases the spectra only display the carbon bands. The most intense bands correspond to the first order bands [44,50] located at 1350 cm^{-1} (D band) and at 1580 cm^{-1} (G band), while the other less intense bands known as second order bands, are located at 2700 cm^{-1} (G′ band) and at 2930 cm^{-1}, (D + G) [51]. Carbon materials with structural defects such as Csp^3 or broken Csp^2 bonds present a high intensity of the D band, while the G band depends on Csp^2 and it is directly related with the degree of order [51]. The I_D/I_G ratio is a parameter widely used to estimate the graphitization index and the degree of order of carbon materials [51]. The position and width (*FWHM* = full width at half maximum) of the D and G bands but, also the intensity of the G' band are related with the graphitization and the type of carbon [51–53].

As it is clearly observed in Fig. 6 and Table 3, the I_D/I_G ratio and the *FWHM* values of the D and G bands increase with the Ni(%) indicating

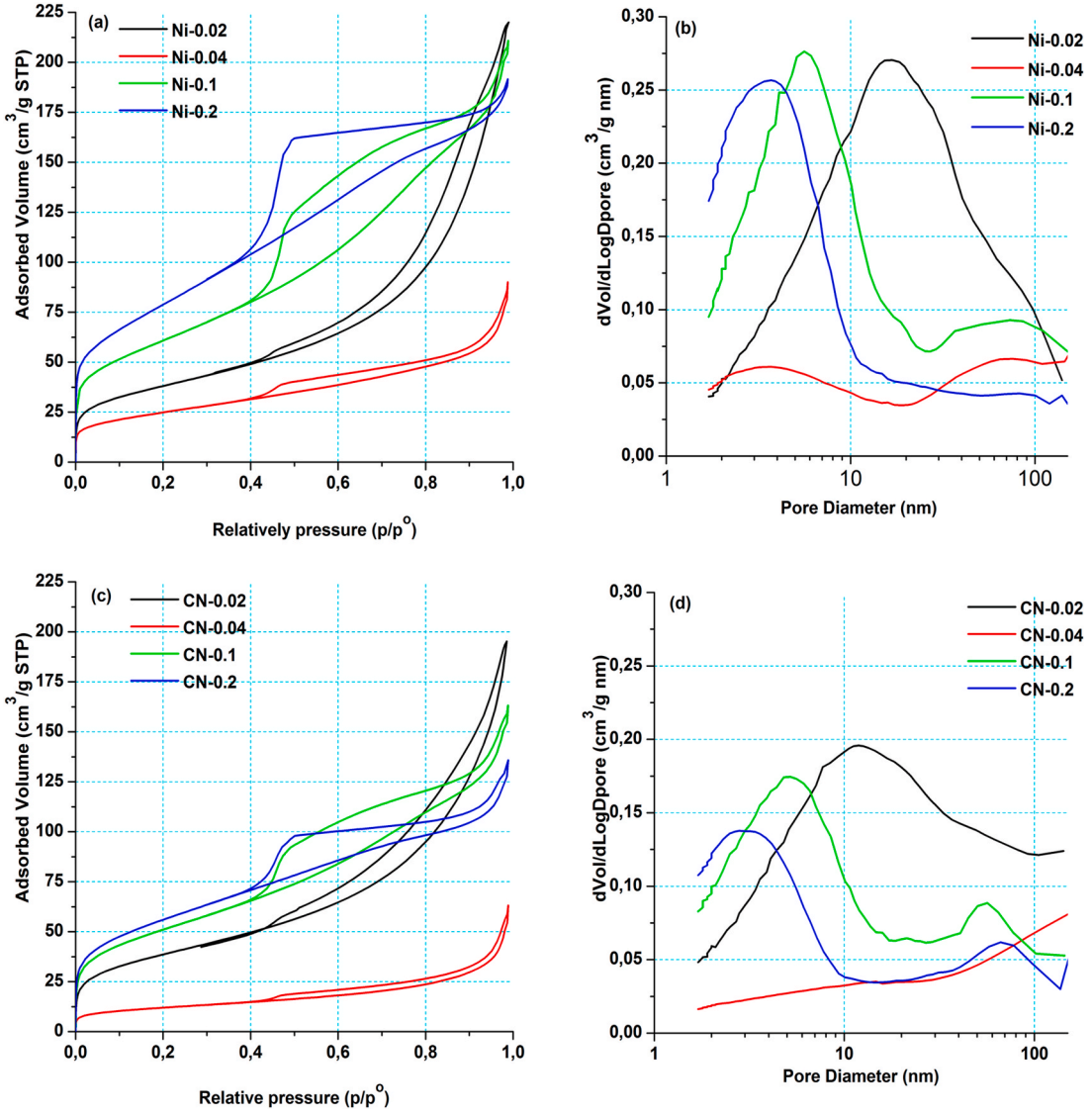

Fig. 4. N_2 isotherms and PSDs of (a), (b) Ni-doped porous glasses and c), (d) related CNFs/glass materials prepared with different Ni(%) after CH_4:N_2 (100:100) treatment at 600 °C (3 h).

that the degree of order of the CNFs decreases. Despite of the very low amount of CNFs for the lowest Ni(%) samples (CN-0.02 and CN-0.01) the Raman spectra are perfectly observed even with the lowest I_D/I_G ratio and, this probably indicates that in those samples highly ordered CNFs must be hidden inside the porous glass support. As the Ni(%) increases (CN-0.1 and CN-0.2), the I_D/I_G varies from 0.2 to 0.8 indicating more defective CNFs. It is important to note that the I_D/I_G results are considerable lower than the ones obtained by several authors (ranged from 0.2 to 1.5) employing CCVD for growing CNFs/CNTs on SiO_2 supports [27,29,32,54] indicating that our CNFs are more ordered.

Other useful parameter to evaluate the formation CNFs is L_a. As Banergee et al. [32] proposed, the increase of defects in the CNFs with the Ni(%) (i.e. I_D/I_G varies from 0.2 to 0.8) could be asigned to the decrease in the L_a domain size (i.e. varies from 22.0 to 5.5 nm). This result is probably ascribed to an increasing number of interconnects and junctions and smaller graphitic crystal size.

In order to evaluate the thermal oxidation resistance of the samples [51], TG analysis was performed under air atmosphere (Fig. 7(a)). The first weight gain (*WG*) occurs from 217 to 251 °C and is assigned to the oxidation of the Ni catalyst to form NiO [49]. This *WG* is only observed in the samples with the highest Ni(%) (i.e. CN-0.1 = −2% and CN-0.2 = −3%). At higher temperatures two weight losses (*WL1* and *WL2*) due to a two-step thermal decomposition are clearly seen in the differential thermogravimetric (DTG) curves (Fig. 7(b)). *WL1* could be due to the oxidation of less graphitic materials such as amorphous carbon (AC) [49], to the condensation of Si–OH groups and also to the degradation of the carbon material with the aid of these Si–OH groups [18]. *WL2* can be assigned to the degradation of high ordered carbon such as CNFs or CNTs. *WL1* occurs from 359 to 384 °C and increases with the amount of the Ni(%) and hence with the C(%), while *WL2* occurs from 523 to 566 °C and displays the same trend. It is important to note that *WL1* +*WL2* exceeds the total amount of the C(%) detected in Table 1. As it was previously stated [34], *WL1* must be somehow related to the presence of some residual Si-OH formed during aqueous processes (i.e. acid leaching and Ni impregnation), which are still present on the surface of the glass support or in its porous structure. Therefore WL1 is related to (1) the condensation of Si–OH groups (Si–OH + Si–OH → Si–O–Si + H_2O) and (2) the degradation of CNFs by the aid of Si–OH or H_2O formed on the surface [18]. The presence of Si–OH groups was observed by ATR analysis (by the presence of a band situated at 950-960 cm^{-1} (Fig. SI 1). Finally, WL2 can be associated to the degradation of less accessible CNFs, i.e. the ones formed inside the porous glass support. All these

Table 2
Summary of N_2 adsorption-desorption experiments of Ni impregnated porous glasses and the related CNFs/glass materials obtained with different Ni(%) and CH_4:N_2 ratio. These results are also compared with the Ni impregnated porous glass thermal treated at 600 °C in air.

Sample	*Surface* (mg^{-1})			*Volume* (cm^3g^{-1})			d_{pore} (nm)
	S_{BET}	S_{mic}	S_{mes}	$V_{mic + mes}$	V_{mic}	V_{mes}	
Ni-0.02	134	14	117	0.34	<0.005	0.31	10.1
Ni-0.04	87	33	54	0.14	0.03	0.11	6.4
Ni-0.1	218	44	174	0.33	<0.005	0.27	6.0
Ni-0.2	286	90	191	0.30	0.08	0.22	4.1
CN-0.02	137	26	109	0.30	<0.005	0.27	8.8
CN-0.04	41	10	26	0.10	<0.005	0.09	9.5
CN-0.1	181	55	122	0.25	0.04	0.20	5.6
CN-0.2	197	84	106	0.22	0.05	0.15	4.4
Ni-0.02-Air	114	12	98	0.36	<0.005	0.33	12.5
Ni-0.04-Air	38	4	32	0.13	<0.005	0.12	13.3
Ni-0.1-Air	200	18	177	0.35	<0.005	0.31	7.1
Ni-0.2-Air	223	33	181	0.27	<0.005	0.21	4.8
CN 100:200	186	79	100	0.18	0.05	0.12	3.9
CN 100:100	197	84	106	0.22	0.05	0.15	4.4
CN 100:50	177	70	100	0.20	0.04	0.15	4.6
CN 100:25	168	67	94	0.19	0.04	0.13	4.5
CN 100:0	155	69	78	0.16	0.04	0.11	4.1

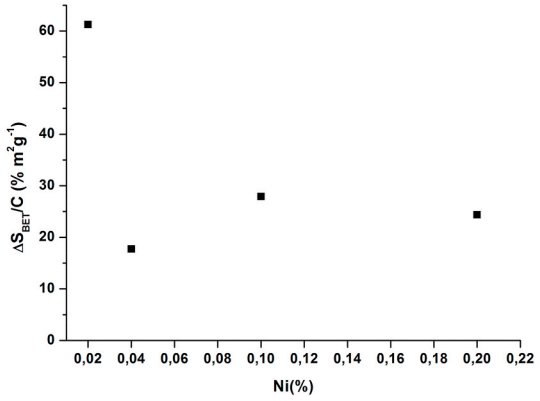

Fig. 5. Evolution of ΔS_{BET}/C(%) of CNFs/glass materials formed employed different Ni(%).

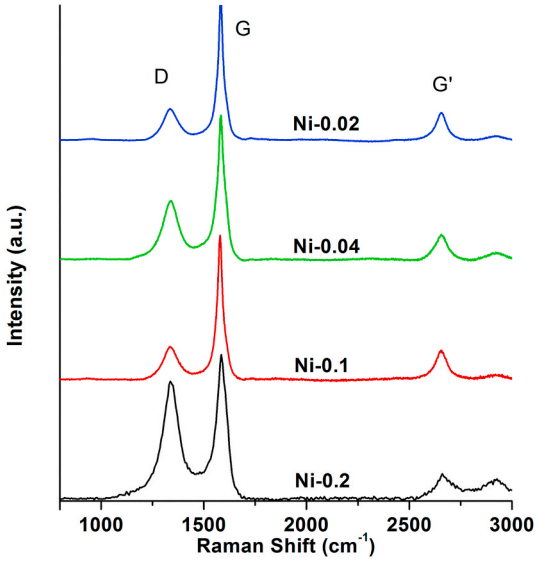

Fig. 6. Raman spectra of CNFs/glass materials prepared with different Ni(%).

Table 3
Summary of Raman results of CNFs/glass materials prepared with different Ni (%).

Sample	D (cm^{-1})	FWHM D (cm^{-1})	G (cm^{-1})	FWHM G (cm^{-1})	I_D/I_G	L_a(nm)
CN-0.02	1336	79	1582	33	0.2	22.0
CN-0.04	1340	89	1583	42	0.4	11.0
CN-0.1	1336	78	1580	35	0.2	22.0
CN-0.2	1340	93	1586	55	0.8	5.5

asumptions perfectly agree with the Ni(%), C(%) (Table 1), FE-SEM (Fig. 3) and N_2 adsorption-desorption (Table 2) results, which indicate that the highest amount of Ni (i.e. Ni-0.2) produces the major formation of CNFs all over the surface and also inside the porous glass matrix.

These CNF/glass materials have been planned to form glass composites with enhanced thermal and electrical properties. In these sense, just taking into account the Ni(%) the best experimental conditions are those where the maximum amount of carbon is obtained, which is the Ni-0.2 composition. Based on this assumption, the *CH_4:N_2 ratio* has been varied only with this composition.

3.2. *Effect of CH_4:N_2 ratio*

As it is clearly observed in Table 4, the carbon content greatly increases in the CNFs/glass materials with the amount of CH_4. Indeed, the carbon content is 35% in the sample prepared only with CH_4 (i.e. 100:0 CH_4:N_2), what is 5 times bigger than the one prepared with the lowest amount of CH_4 (i.e. 100:200 CH_4:N_2). These results are quite obvious taking into account that CH_4 is used as carbon source, so higher amounts of CH_4 produce more carbon deposition in tubular form such as CNFs.

The FE-SEM micrographs showed in Fig. 8 are in line with the C(%) displayed in Table 4. As it is evident the amount of CNFs greatly increases as CH_4:N_2 ratio decreases. This fact is especially noticeable in the case of the CN 100:0 sample which has the highest amount of carbon (C = 35.7%). Large, homogeneous and well-dispersed entanglements of CNFs are covering the sample surface but also filling the pores of the glass matrix. CNFs are quite long (at least several μm) and display homogeneous diameter but, as the amount of carbon source increases the diameter slightly increases from 25 to 30 nm (Table 4 and Fig. 8). Furthermore, the length and quantity are widely enhanced. These differences can be perfectly evaluated when CN 00:200 and CN 100:0 samples are compared.

As it has been explained before, the evolution of the porosity is directly related with the formation of CNFs in the porous glass support and depends on the experimental conditions. In this sense, N_2 adsorption-desorption measurements were carried out for these CNFs/glass materials (Fig. 9 and Table 2). These data are also compared with those of the pristine porous glass impregnated with Ni (Ni-0.2) before and after the thermal treatment at 600 °C in air atmosphere.

The Ni-0.2 sample displays a type IVa isotherm, with a H2a hysteresis loop related to *ink-bottle* mesopores with a PSDs of 4.1 nm of mean diameter (Table 2), where pore necks are very narrow [47] (Fig. 9). When this sample is treated at 600 °C in air the isotherm shows a lower adsorption volume, due to the elimination of pores of lower sizes, i.e. the micropores and small-size mesopores (Table 2). However, after the thermal treatment under different CH_4:N_2 ratio, although the type and shape of the isotherms are maintained, the N_2 adsorbed volumes continuously decrease. That decrease can be associated, in terms of porosity, to the progressively filling of the pores of the glass support and the formation of new ones as a consequence of the growth of CNFs [34] (Fig. 9). Those changes are in agreement with the C(%) (Table 4) and FE-SEM images (Fig. 8) indicating the increase of the amount of CNFs with the CH_4 concentration. Pore filling due to the growth of CNFs leads to a decrease of the surface area and pore volume values as it is observed

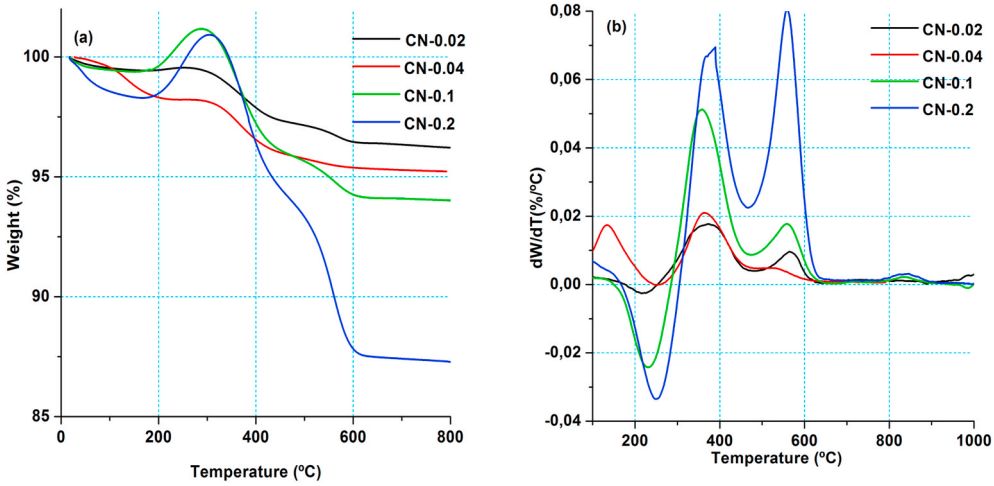

Fig. 7. (a) TG and (b) DTG curves of CNFs/glass materials obtained employing different Ni(%).

Table 4
Summary of Ni(%), C(%) and CNFs diameter for CNFs/glass materials obtained with different CH_4:N_2 ratio.

Sample	CH_4:N_2	Ni(%)	C(%)	CNFs diameter (nm)
CN 100:200	100:200	17.8	6.9	25 ± 6
CN 100:100	100:100	17.8	8.0	27 ± 6
CN 100:50	100:50	17.8	13.5	27 ± 6
CN 100:25	100:25	17.8	17.8	27 ± 7
CN 100:0	100:0	17.8	35.7	30 ± 6

in Table 2. S_{BET} varies from 286 to 155 m^2g^{-1} which undoubtedly indicates the progressive filling of the pores of the glass support with the CNFs. Taking into account the evolution of S_{mic} and S_{meso} that filling mainly occurs in mesopores (S_{mic} varies from 90 to 69 m^2g^{-1} and S_{meso} varies from 191 to 78 m^2g^{-1} from Ni-0.2 to CN 100:0). This could indicate that the Ni particles are mainly located inside the mesoporous as we stated before. The PSD in Fig. 9(b) displays how the volume of the pores related to the glass support (≈4 nm) is progressively reduced, while new bigger pores, around 60–70 nm, appear. These new pores may be formed between the large entanglements of CNFs [48], and they appear in the samples from 100:100 to 100:25 CH_4:N_2 ratio. It must be noticed, that in the case of the CNF 100:0 sample the diameter of the pores shifts to 20 nm, probably indicating larger entanglements of CNFs in those experimental conditions (i.e. CH_4:N_2 100:0).

The method of formation of CNFs reported in this work differs from other ones [25] such as that of CNTs/Al_2O_3 materials where was observed the increase of S_{BET} when CNTs are formed, indicating the formation of CNTs over the support surface. However, in our case the formation of CNFs is quite different. First, in the method we propose here, we can select the pore size of the pristine porous glass in accordance with the *Vycor* process, after that the catalyst is homogeneously deposited over the surface and also inside of pores and, finally depending on the experimental conditions (CH_4:N_2 ratio and Ni(%)) CNFs are formed. In all the cases, as the amount of carbon increases, S_{BET} decreases undoubtedly indicating that CNFs are formed all over the surface and also inside the porous support. This fact is also corroborated by the FE-SEM images (Fig. 8) which indicate that the CNFs are located on the surface but also emerging from porous glass support. In summary, the Ni particles are located inside smaller pores (mainly in mesopores due to the difficult micropore accessibility) but also inside macropores and over external surface. This is in accordance with the bimodal PSD found in the samples, where first the reduction in both size and amount of initial mesopores (around 4 nm) can be associated to the CNFs formed inside the smaller pores and, second the large mesopores (20–80 nm) are associated to large entanglements of CNFs when filling pores but also to those CNFs formed over the external surface.

As it was commented above, $\Delta S_{BET}/C(\%)$ can be used as a estimation of the features of the bundles of CNFs, where low values indicate small CNFs diameter and low carbon amount deposited in tubular form [49]. Based on these asumptions it seems clear that as the amount of CH_4 increases the $\Delta S_{BET}/C(\%)$ of CNFs decreases (see Fig. 10). Therefore, if the amount of CNFs were not considered, the optimal experimental conditions in terms of CNFs quality would be those for CH_4:N_2 ratio of 100:200 and 100:100.

The C(%) (Table 4), FE-SEM (Fig. 8) and N_2 adsorption-desorption (Fig. 9 and Table 2) results indicate the great influence of the CH_4:N_2 ratio in the quantity, length and diameter of the CNFs formed. These CNFs features can be controlled just varing these parameters. The decomposition of CH_4 and the subsequent deposition of carbon in the form of CNFs are favoured as the flow of N_2 decreases. However, other aspects such as degree of order and thermal estability for the formed CNFs must be also known. Raman spectra and their main results of the CNFs/glass materials obtained for different CH_4:N_2 ratio are collected in Fig. 11 and Table 5, respectively.

Table 5 shows a great correlation between the CH_4:N_2 ratio and the graphitization index. In accordance with the increase of both *FWHM* of G band and the I_D/I_G ratio (which varies from 0.7 to 1.4) it must be concluded that the order degree of the CNFs decrease with the amount of CH_4. These values are somehow similar to those found in the literature where the CCVD method is used to grow CNFs/CNTs employing CH_4 as carbon source and Ni as catalyst [27,29,32,54]. The increase of I_D/I_G with the amount of CH_4, is also related to L_a which decreases from 6.3 to 3.1 nm. The more defective CNFs the more number of interconnects and junctions and, therefore smaller graphitic crystal sizes [32].

On the other hand, the changes related to the carbon content can be explained in terms of the thermal decomposition of CH_4 under Ni catalysts ($CH_4 \rightarrow 2H_2 + C$), somehow probably due to a base-growth mechanism and the great interaction between the support and the catalyst [31]. So, the increase of the CH_4 amount does not produce the passivation of Ni during the deposition of carbon over the active catalyst sites, instead the CH_4 generates thicker and longer CNFs. The growth mechanism occurs in several stages [55]: (1) Ni produces the decomposition of CH_4 into H_2 and C, (2) then occurs the dissolution and diffusion of the carbon particles throught the Ni sites, (3) CNFs are precipitated over the other side of the Ni catalyst and do not cover catalyst preventing its passivation. There are some points which can explain why as CH_4 increases also the amount of CNFs does, with no evident sings of catalyst passivation. The first one is the low reactivity of CH_4, the catalytic decomposition of CH_4 must produce few amounts of

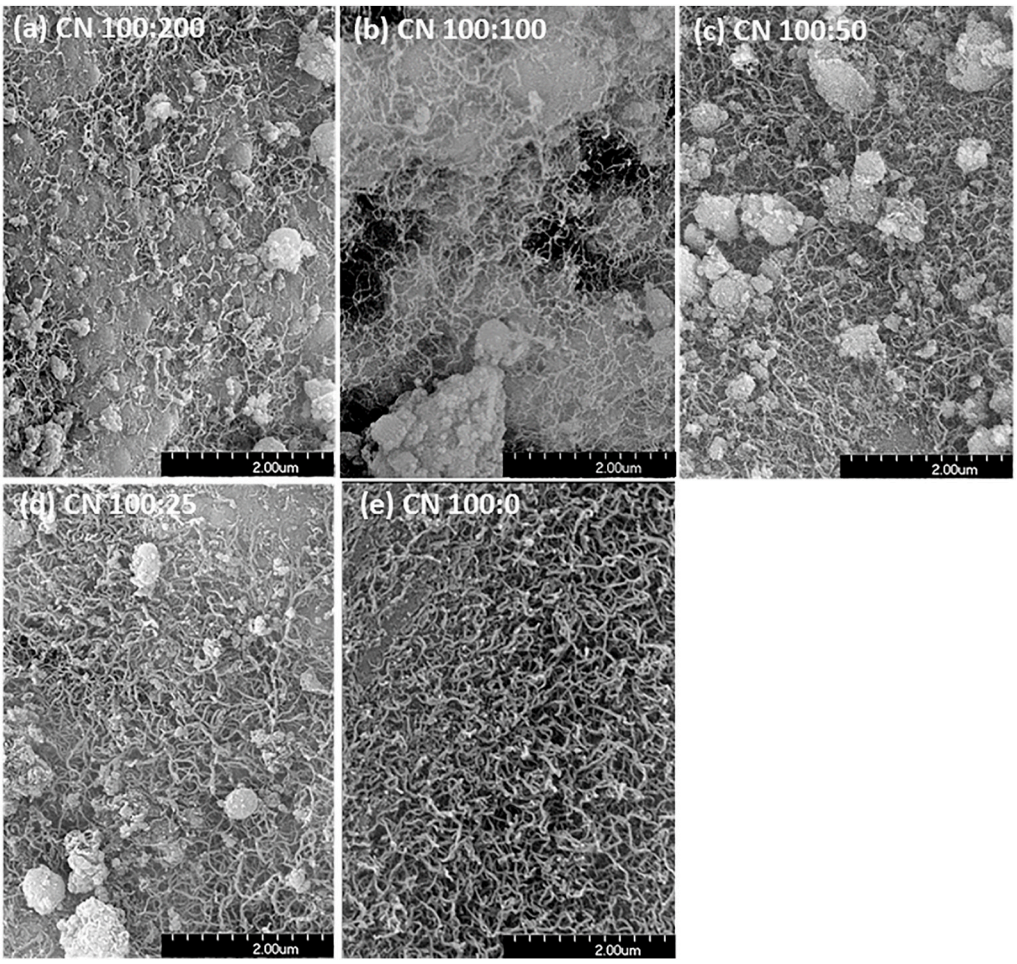

Fig. 8. FE-SEM micrograps of CNFs/glass materials prepared with different CH_4:N_2 ratio: (a) 100:200, (b) 100:100, (c) 100:50 (d) 100:25 and (e) 100:0.

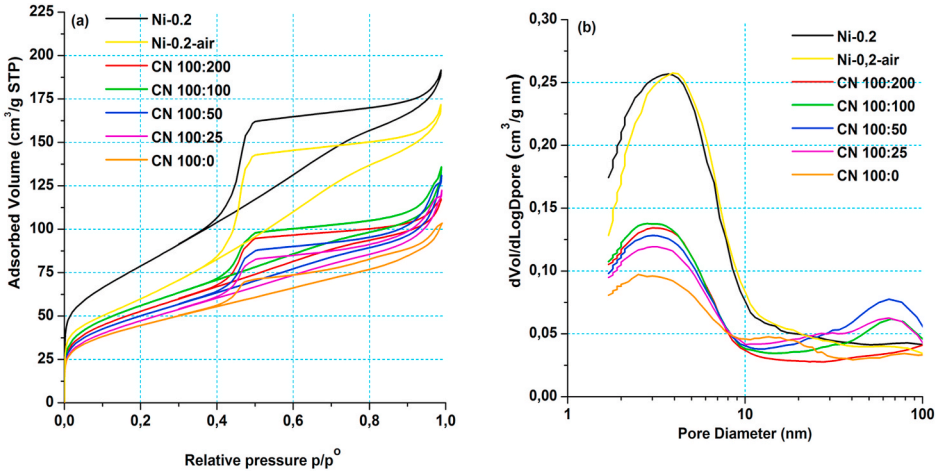

Fig. 9. a) N_2 adsorption-desorption isotherms and b) PSDs of CNFs/glass materials prepared with different CH_4:N_2 ratio.

carbon even with the highest CH_4 flow giving enough time to form the CNFs. This fact does not occur for other high reactive carbon sources as ethylene which passivates the catalyst and does not produce CNFs, needing the presence of H_2 which decreases the catalyst passivation [29]. The second one is that the Ni particles are anchored to the porous glass support and the CNFs are formed over the Ni surface. In the case of the highest amount of CH_4, the flow facilitates the formation and also the movement of the CNFs far away from the Ni particles preventing their passivation. As *Ju* et al. [30] stated, the catalyst-support interactions determine the growth mechanism. Weak interactions produce a tip-growth mechanism, characteristic of conventional catalyst systems coordinated by van der Waals forces [33].The CH_4 decomposes over the catalyst and carbon diffuses toward the downside of the catalyst. Strong interactions favor a base-growth mechanism. The metal particles are anchored to the support and the CNFs are not able to push away the catalyst and they have to emerge from the support.

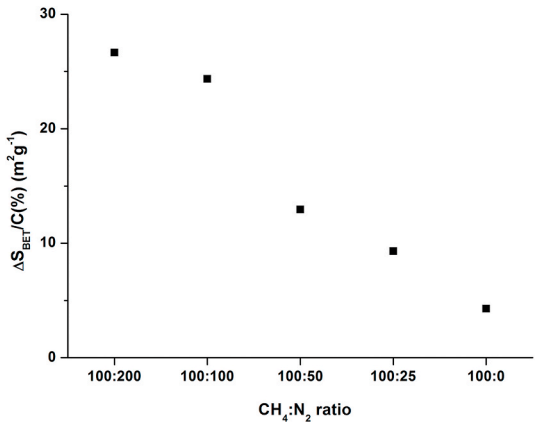

Fig. 10. Evolution of $\Delta S_{BET}/C(\%)$ of CNFs/glass materials formed employed different CH_4:N_2 ratio.

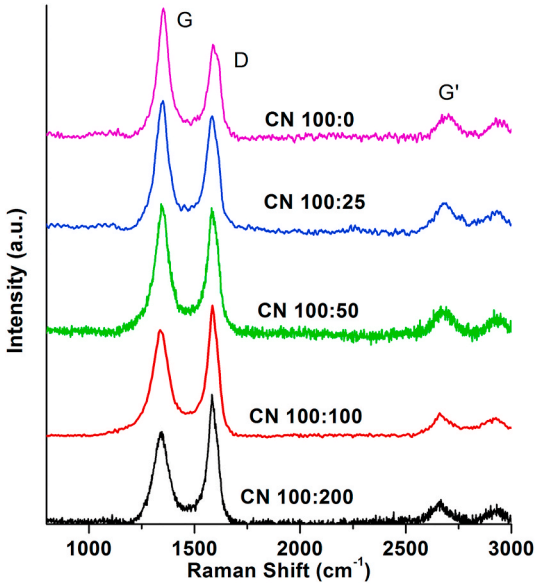

Fig. 11. Raman spectra of CNFs/glass materials prepared at different CH_4:N_2 ratio.

Table 5
Summary of Raman results of CNFs/glass materials prepared with different CH_4:N_2 ratio at 600 °C (3 h).

$CH_4:N_2$	D (cm^{-1})	*FWHM* D (cm^{-1})	G (cm^{-1})	*FWHM* G (cm^{-1})	I_D/I_G	L_a(nm)
100:200	1351	81	1583	53	0.7	6.3
100:100	1340	93	1586	55	0.8	5.5
100:50	1349	80	1582	60	1.0	4.4
100:25	1351	71	1583	65	1.1	4.0
100:0	1353	63	1588	61	1.4	3.1

In the tip-growth mechanism, the deactivation of the Ni catalyst occurs by the deposition of certain amount of carbon at the tips of the CNFs [27]. In the case of the base-growth mechanism, the metal particles remain on the glass and this fact does not occur, offering new and very interesting possibilities of these materials, for example enhancing the time of catalytic life of Ni and so the formation of CNFs and CO_x-free H_2 [30]. Similar results of base-growth CNTs have been obtained over the Fe/SiO_2 system employing acetylene as carbon source [31] and in bimetallic catallyst (9Ni–1Co) supported over Al_2O_3 and TiO_2–Al_2O_3 via the CCVD of metane [33].

TG and DTG curves collected under air atmosphere of the CNFs/glass materials obtained employing different CH_4/N_2 flow are showed in Fig. 12(a) and (b), respectively. The samples present three different processes. An initial *WG* from 251 to 282 °C asigned to the Ni oxidation [49]. Two *WLs* (*WL1* and *WL2*) related to a two-step thermal degratation of the CNFs/glass materials appear at higher temperatures. *WL1* occurs from 361 to 384 °C and *WL2* occurs from 551 to 581 °C. As occurred before for the samples obtained with different Ni(%), *WL1* + *WL2* exceeds the total amount of C(%) (Table 4). *WL1* is rather similar in all the cases, but a slightly decreases is observed for the sample when the highest amount of CH_4 was employed (CN 100:0) (*WL1* varies from 6 to 2%). However, *WL2* increases with the CH_4 content, and hence with the amount of C(%) and CNFs in the materials. As it was proposed in the case of the CNFs/glass materials with different Ni(%), *WL1* must be due to the condensation of the Si–OH groups and also to the degradation of the CNFs induced by these highly reactive groups mainly on the surface [34]. The presence of the Si–OH groups on the surface of these materials have been corroborated by the ATR spectra (Fig. SI 2) with the presence of a 950-960 cm^{-1} band. Furthermore, the huge increase of the CNFs (i.e. the amount (C(%)) varies from 6.7 to 35.7%, the length, the diameter (Table 4 and Fig. 8) and the less amount of Si–OH groups (Fig. SI 2) could partially hinder the degration of the CNFs explaining the decrease observed in *WL1* from 7 to 2%. *WL2* is related to the degradation of the less accessible CNFs, and probably those located inside the pores. The maximum temperature of *WL2* varies from 551 to 581 °C, as the amount of CH_4 increases, this displacement can also be explained with the huge increase of the CNFs (amount, length and diameter) observed [56].

In summary, both the Ni(%) and CH_4:N_2 ratio determine the amount, length, diameter, morphology, degree of order and thermal stability of the CNFs obtained within a mesoporous glass and therefore, they also influence the porosity of the related CNFs/glass materials. In this sense, a precise selection of these parameters will allow us to prepare CNFs/glass materials with specific tuned properties which have to be in consonance for the specific requirements of the final applications.

4. Conclusions

CNFs/glass materials have been obtained by the CCVD process of CH_4 employing Ni catalyst supported on a porous glass. The effect of the amount of the catalyst (i.e. Ni (%)) and carbon source (i.e. CH_4:N_2 ratio) were determined. As the amount of catalyst and carbon source increases, the quantity (from 2.2 up to 35.7 of C(%)), length (<500 nm up to several μm) and diameter (from 24 to 30 nm) of the *in situ* growth CNFs are enhanced, but the order degree (I_D/I_G varies from 0.2 to 1.4) and L_a (from 22.0 to 3.1 nm) decrease progressively. The CNFs observed are *bamboo-like* and *fish-bone* with hollow core, both with open ends which increase their chemical activity being interesting for novel applications in the field of the medicine among others. During the CNFs formation the Ni catalyst is observed anchored to the glass support, which indicates a strong interaction between the catalyst and the support denoting a base-growth mechanism. This mechanism is a very interesting way to produce large amounts of CNFs without producing the deactivation of the catalyst sites for long times.

During the CCVD process, as the amount of CNFs increases, porosity parameters mainly S_{BET}, V_{mes} and S_{mes} decrease progressively indicating the filling of the mesopores. New pores of 20–70 nm appear which are associated to large bundles of CNFs formed during the filling of the mesopores. This indicates, taking into account the incipient densification experienced by the glass support at 600 °C, that more CNFs are placed in less volume which lead to the formation of more interconnections and junctions, explaining the formation of a high defective CNFs with lower L_a domains.

To the best of our knowledge there have not been previous studies which indicate a base-growth mechanism in the Ni/glass system by the CCVD process of CH_4. These findings offer very interesting applications in the production of CNFs and CO_x-free H_2 employing a relatively low

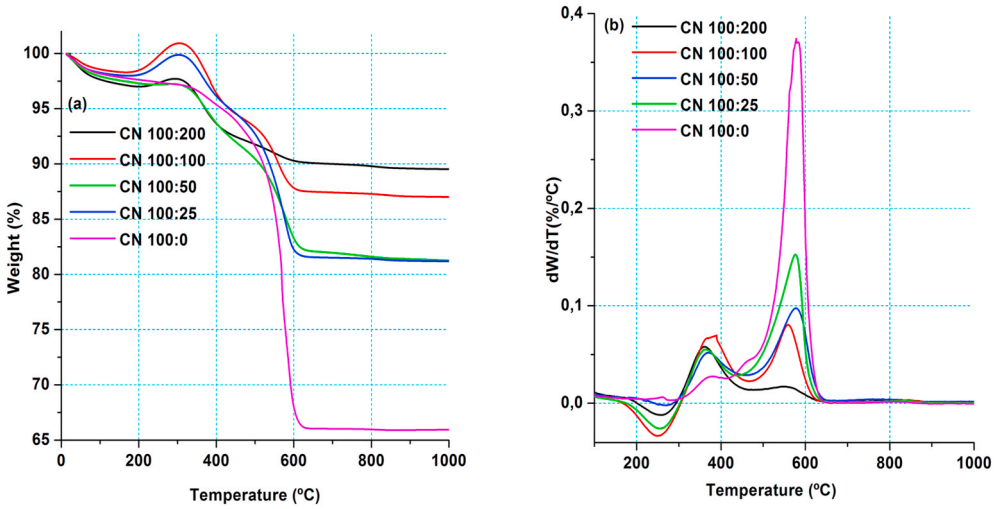

Fig. 12. (a) TG and (b) DTG curves of CNFs/glass materials prepared at different CH_4:N_2 ratio.

temperature (600 °C) for long times (3 h) and, also a cheap Ni/glass catalytic system. All these facts demonstrate the suitability of this process with scalable possibilities in the field of catalyst and energy very demanding nowadays. Finally, the obtained CNFs/glass materials can be potentially used in many fields as electronic devices, catalyst and biocatalyst systems, energy storage materials, etc.

Declaration of competing interest

The authors declare that they have no known competing financial interests or personal relationships that could have appeared to influence the work reported in this paper.

Acknowledgements

This work was supported by project MAT2016-78700-R financed by Spanish Research Agency and European Regional Development Fund (AEI/FEDER, EU).

Appendix A. Supplementary data

Supplementary data to this article can be found online at https://doi.org/10.1016/j.micromeso.2021.111168.

Credit author statement

M.A.M: Conceptualization, Supervision, Writing – review and editing, J.S: Investigation, Methodology, Writing – original draft, I.M.-G.: Investigation, Writing – review and editing J.R: Conceptualization, Supervision, Writing – review and editing, Funding acquisition.

References

[1] S. Iijima, Helical microtubules of graphitic carbon, Nature 354 (6348) (1991) 56–58.
[2] S. Iijima, T. Ichihashi, Single-shell carbon nanotubes of 1-nm diameter, Nature 363 (6430) (1993) 603–605.
[3] J. Cho, A.R. Boccaccini, M.S.P. Shaffer, Ceramic matrix composites containing carbon nanotubes, J. Mater. Sci. 44 (8) (2009) 1934–1951.
[4] S.C. Tjong, Carbon Nanotube Reinforced Composites: Metal and Ceramic Matrices, 2009.
[5] E. Zapata-Solvas, D. Gómez-García, A. Domínguez-Rodríguez, Towards physical properties tailoring of carbon nanotubes-reinforced ceramic matrix composites, J. Eur. Ceram. Soc. 32 (12) (2012) 3001–3020.
[6] A.A. Silva, R.A. Pinheiro, A.C. Rodrigues, M.R. Baldan, V.J. Trava-Airoldi, E. J. Corat, Graphene sheets produced by carbon nanotubes unzipping and their performance as supercapacitor, Appl. Surf. Sci. 446 (2018) 201–208.
[7] E. Zhang, J. Wang, B. Wang, X. Yu, H. Yang, B. Lu, Unzipped carbon nanotubes for aluminum battery, Energy Stor. Mater. 23 (2019) 72–78.
[8] O.V. Perlova, Y.S. Dzyazko, A.V. Palchik, I.S. Ivanova, N.O. Perlova, M.O. Danilov, I.A. Rusetskii, G.Y. Kolbasov, A.G. Dzyazko, Composites based on zirconium dioxide and zirconium hydrophosphate containing graphene-like additions for removal of U(VI) compounds from water, Appl. Nanosci. 10 (12) (2020) 4591–4602.
[9] C. Palencia, M.A. Mazo, A. Nistal, F. Rubio, J. Rubio, J.L. Oteo, Processing and properties of carbon nanofibers reinforced epoxy powder composites, J. Nanoparticle Res. 13 (11) (2011) 6021–6034.
[10] S.R. Bakshi, D. Lahiri, A. Agarwal, Carbon nanotube reinforced metal matrix composites - a review, Int. Mater. Rev. 55 (1) (2010) 41–64.
[11] M.A. Mazo, A. Tamayo, A.C. Caballero, J. Rubio, Enhanced electrical and thermal conductivities of silicon oxycarbide nanocomposites containing carbon nanofibers, Carbon 138 (2018) 42–51.
[12] C. Zheng, M. Feng, Y. Du, H. Zhan, Synthesis and third-order nonlinear optical properties of a multiwalled carbon nanotube-organically modified silicate nanohybrid gel glass, Carbon 47 (12) (2009) 2889–2897.
[13] M.J. de Andrade, A. Weibel, C. Laurent, S. Roth, C.P. Bergmann, C. Estournès, A. Peigney, Electrical conductive double-walled carbon nanotubes - silica glass nanocomposites prepared by the sol-gel process and spark plasma sintering, Scripta Mater. 61 (10) (2009) 988–991.
[14] H. Yuan, H.Y. Liu, J.Y. Diao, X.M. Gu, D.S. Su, Supported carbon nanotubes on SiO_2 spheres as robust monolithic catalysts for the oxidative dehydrogenation of ethylbenzene, Xinxing Tan Cailiao/New Carbon Mater. 28 (5) (2013) 336–341.
[15] G.A. Kovalenko, A.B. Beklemishev, L.V. Perminova, A.L. Mamaev, N.A. Rudina, S. I. Moseenkov, V.L. Kuznetsov, Immobilization of recombinant E. coli thermostable lipase by entrapment inside silica xerogel and nanocarbon-in-silica composites, J. Mol. Catal. B Enzym. 98 (2013) 78–86.
[16] L. Zhou, S. Pan, X. Chen, Y. Zhao, B. Zou, M. Jin, Kinetics and thermodynamics studies of pentachlorophenol adsorption on covalently functionalized Fe_3O_4atSiO_2-MWCNTs core-shell magnetic microspheres, Chem. Eng. J. 257 (2014) 10–19.
[17] H. Parham, S. Bates, Y. Xia, Y. Zhu, A highly efficient and versatile carbon nanotube/ceramic composite filter, Carbon 54 (2013) 215–223.
[18] M.A. Mazo, C. Palencia, A. Nistal, F. Rubio, J. Rubio, J.L. Oteo, Microstructure of low temperature processed CNFs/glass nanocomposites, J. Mater. Sci. 47 (13) (2012) 5169–5180.
[19] A.R. Boccaccini, D.R. Acevedo, G. Brusatin, P. Colombo, Borosilicate glass matrix composites containing multi-wall carbon nanotubes, J. Eur. Ceram. Soc. 25 (9) (2005) 1515–1523.
[20] B.T.T. Chu, G. Tobias, C.G. Salzmann, B. Ballesteros, N. Grobert, R.I. Todd, M.L. H. Green, Fabrication of carbon-nanotube-reinforced glass-ceramic nanocomposites by ultrasonic in situ sol-gel processing, J. Mater. Chem. 18 (44) (2008) 5344–5349.
[21] M.J. De Andrade, M.D. Lima, C.P. Bergmann, G.D.O. Ramminger, N.M. Balzaretti, T.M.H. Costa, M.R. Gallas, Carbon nanotube/silica composites obtained by sol-gel and high-pressure techniques, Nanotechnology 19 (26) (2008).
[22] F.C. Dillon, J. Moghal, A. Koós, J.G. Lozano, L. Miranda, H. Porwal, M.J. Reece, N. Grobert, Ceramic composites from mesoporous silica coated multi-wall carbon nanotubes, Microporous Mesoporous Mater. 217 (2015) 159–166.
[23] G. Tao, S. Chen, S.J. Pandey, F.A. Tan, H. Ebendorff-Heidepriem, M. Molinari, A. F. Abouraddy, R.M. Gaume, A carbon-nanofiber glass composite with high electrical conductivity, Int. J. Appl. Glass Sci. (2019).
[24] F. Ghaemi, M. Ali, R. Yunus, R.N. Othman, Chapter 1 - synthesis of carbon nanomaterials using catalytic chemical vapor deposition technique, in: S.A. Rashid, R.N.I. Raja Othman, M.Z. Hussein (Eds.), Synthesis, Technology and Applications of Carbon Nanomaterials, 2019, pp. 1–27. Elsevier.

[25] A. Peigney, C. Laurent, O. Dumortier, A. Rousset, Carbon nanotubes–Fe–alumina nanocomposites. Part I: influence of the Fe content on the synthesis of powders, J. Eur. Ceram. Soc. 18 (14) (1998) 1995–2004.
[26] C. Laurent, A. Peigney, O. Dumortier, A. Rousset, Carbon nanotubes–Fe–Alumina nanocomposites. Part II: microstructure and mechanical properties of the hot-Pressed composites, J. Eur. Ceram. Soc. 18 (14) (1998) 2005–2013.
[27] S. Takenaka, S. Kobayashi, H. Ogihara, K. Otsuka, Ni/SiO2 catalyst effective for methane decomposition into hydrogen and carbon nanofiber, J. Catal. 217 (1) (2003) 79–87.
[28] E. Miniach, A. Śliwak, A. Moyseowicz, G. Gryglewicz, Growth of carbon nanofibers from methane on a hydroxyapatite-supported nickel catalyst, J. Mater. Sci. 51 (11) (2016) 5367–5376.
[29] O.A. Aberefa, M.O. Daramola, S.E. Iyuke, Production and functionalization of carbon nanotubes for application in membrane synthesis for natural gas separation, Microporous Mesoporous Mater. 280 (2019) 26–36.
[30] D. Ayillath Kutteri, I.W. Wang, A. Samanta, L. Li, J. Hu, Methane decomposition to tip and base grown carbon nanotubes and COx-free H2 over mono- and bimetallic 3d transition metal catalysts, Catal. Sci. Technol. 8 (3) (2018) 858–869.
[31] S.A. Shokry, A.K. El Morsi, M.S. Sabaa, R.R. Mohamed, H.E. El Sorogy, Study of the productivity of MWCNT over Fe and Fe–Co catalysts supported on SiO2, Al2O3 and MgO, Egyptian J. Pet. 23 (2) (2014) 183–189.
[32] P.C. Banerjee, D.E. Lobo, T. Williams, M. Shaibani, M.R. Hill, M. Majumder, Graphitic carbon nanofiber growth from catalytic-metal organic frameworks & their electrochemical double layer properties, J. Mater. Chem. 5 (48) (2017) 25338–25349.
[33] B. Gao, I.W. Wang, L. Ren, J. Hu, Catalytic methane decomposition over bimetallic transition metals supported on composite aerogel, Energy Fuels 33 (9) (2019) 9099–9106.
[34] M.A. Mazo, J. Sanguino, A. Tamayo, J. Rubio, Carbon nanofibers grown in situ on porous glass, J. Nano Res. 50 (2017) 1–17.
[35] O.V. Mazurin, E.A. Poraĭ-Koshits, N.S. Andreev, Phase Separation in Glass, 1984. North-Holland.
[36] H. Tanaka, T. Yazawa, K. Eguchi, H. Nagasawa, N. Matsuda, T. Einishi, Precipitation of colloidal silica and pore size distribution in high silica porous glass, J. Non-Cryst. Solids 65 (2) (1984) 301–309.
[37] D. Enke, F. Janowski, W. Schwieger, Porous glasses in the 21st century—a short review, Microporous Mesoporous Mater. 60 (1) (2003) 19–30.
[38] V.A. Kreisberg, V.P. Rakcheev, T.V. Antropova, Influence of the acid concentration on the morphology of micropores and mesopores in porous glasses, Glass Phys. Chem. 32 (6) (2006) 615–622.
[39] G. Toquer, C. Delchet, M. Nemec, A. Grandjean, Effect of leaching concentration and time on the morphology of pores in porous glasses, J. Non-Cryst. Solids 357 (6) (2011) 1552–1557.
[40] S. Brunauer, P.H. Emmett, E. Teller, Adsorption of gases in multimolecular layers, J. Am. Chem. Soc. 60 (2) (1938) 309–319.
[41] E.P. Barrett, L.G. Joyner, P.P. Halenda, The determination of pore volume and area distributions in porous substances. I. Computations from nitrogen isotherms, J. Am. Chem. Soc. 73 (1951) 373–380.
[42] S. Lowell, J. Shields, M. Thomas, M. Thommes, Characterization of Porous Solids and Powders: Surface Area, Pore Size and Density, 2006.
[43] W.D. Harkins, G. Jura, Surfaces of solids. Xiii. A vapor adsorption method for the determination of the area of a solid without the assumption of a molecular area, and the areas occupied by nitrogen and other molecules on the surface of a solid, J. Am. Chem. Soc. 66 (8) (1944) 1366–1373.
[44] F. Tuinstra, J.L. Koenig, Raman spectrum OF graphite, J. Chem. Phys. 53 (3) (1970) 1126–1130.
[45] N.M. Rodriguez, A review of catalytically grown carbon nanofibers, J. Mater. Res. 8 (12) (1993) 3233–3250.
[46] I. Gonzalez, J.C. De Jesus, E. Cañizales, B. Delgado, C. Urbina, Comparison of the surface state of Ni nanoparticles used for methane catalytic decomposition, J. Phys. Chem. C 116 (40) (2012) 21577–21587.
[47] M. Thommes, K. Kaneko, A. Neimark, J. Olivier, F. Rodriguez-Reinoso, J. Rouquerol, K. Sing, Physisorption of gases, with special reference to the evaluation of surface area and pore size distribution (IUPAC Technical Report), Pure Appl. Chem. 87 (2015).
[48] Q.H. Yang, P.X. Hou, S. Bai, M.Z. Wang, H.M. Cheng, Adsorption and capillarity of nitrogen in aggregated multi-walled carbon nanotubes, Chem. Phys. Lett. 345 (1–2) (2001) 18–24.
[49] C. Laurent, A. Peigney, A. Rousset, Synthesis of carbon nanotube–Fe-Al2O3 nanocomposite powders by selective reduction of different Al1.8Fe0.2O3 solid solutions, J. Mater. Chem. 8 (5) (1998) 1263–1272.
[50] D.S. Knight, W.B. White, Characterization of diamond films by Raman spectroscopy, J. Mater. Res. 4 (2) (1989) 385–393.
[51] E. Boccaleri, A. Arrais, A. Frache, W. Gianelli, P. Fino, G. Camino, Comprehensive spectral and instrumental approaches for the easy monitoring of features and purity of different carbon nanostructures for nanocomposite applications, Mater. Sci. Eng. B: Solid-State Mater. Adv. Technol. 131 (1–3) (2006) 72–82.
[52] P. Lespade, A. Marchand, M. Couzi, F. Cruege, Caracterisation de materiaux carbones par microspectrometrie Raman, Carbon 22 (4–5) (1984) 375–385.
[53] M.A. Mazo, A. Tamayo, J. Rubio, Advanced silicon oxycarbide-carbon composites for high temperature resistant friction systems, J. Eur. Ceram. Soc. 36 (10) (2016) 2443–2452.
[54] M.K. Tabatabaei, H.G. Fard, J. Koohsorkhi, Low-temperature growth of vertically aligned carbon nanotubes on a glass substrate using low power PECVD, J. Nano Res. 27 (2014) 163–171.
[55] M. Meyyappan, Carbon Nanotubes: Science and Applications, 2004.
[56] B.J. Landi, C.D. Cress, C.M. Evans, R.P. Raffaelle, Thermal oxidation profiling of single-walled carbon nanotubes, Chem. Mater. 17 (26) (2005) 6819–6834.